Quantitative SPECT Brain Imaging: Effects of Attenuation and Detector Response

D. R. Gilland, R. J. Jaszczak, J. E. Bowsher, T. G. Turkington, Z. Liang, K. L. Greer, and R. E. Coleman

Abstract—**Two physical factors that substantially degrade quantitative accuracy in SPECT imaging of the brain are attenuation and detector response. In addition to the physical factors, random noise in the reconstructed image can greatly affect the quantitative measurement. The purpose of this work was to implement two reconstruction methods that compensate for attenuation and detector response, a 3D maximum likelihood-EM method (ML) and a filtered backprojection method (FB) with Metz filter and Chang attenuation compensation, and compare the methods in terms of quantitative accuracy and image noise. The methods were tested on simulated data of the 3D Hoffman brain phantom. The simulation imcorporated attenuation and distance-dependent detector response. Bias and standard deviation of reconstructed voxel intensities were measured in the gray and white matter regions. The results with ML showed that in both the gray and white matter regions as the number of iterations increased, bias decreased and standard deviation increased. Similar results were observed with FB as the Metz filter power increased. In both regions, ML had smaller standard deviation than FB for a given bias. Reconstruction times for the ML method have been greatly reduced through efficient coding, limited source support, and by computing attenuation factors only along rays perpendicular to the detector.**

I. Introduction

ACCURATE SPECT quantitation of radioisotope concentration in the brain requires compensation for the physical effects of attenuation and detector response. The latter effect is especially important in SPECT brain imaging due to the relatively small size of the structures of interest. In addition to the physical effects, random noise can substantially affect quantitative measurements, and this effect also is more pronounced in smaller regions-of-interest. Although there exists a large body of work related to attenuation and detector response compensation for general SPECT [1]–[15], relatively little work has focused on compensation techniques specifically designed and evaluated for SPECT brain imaging [16]. The objective of this work was to compare two SPECT reconstruction methods which compensate for attenuation and detector response, a filtered backprojection method (FB) and a 3D maximum likelihood-EM (ML) [17], [18], in terms of absolute quantitative accuracy and image noise in reconstructed SPECT brain images.

The problem with evaluating quantitative accuracy and noise in ML or FB reconstruction is that both accuracy and noise can vary with parameters of the reconstruction. Studies with ML have shown that as the number of iterations increases, and resolution and contrast improve, noise increases in the reconstructed images [19], [20]. A similar effect occurs with FB as the filter cut-off, or similar parameter, increases. This study examines ML and FB over a range of the respective reconstruction parameter allowing a comparison of the two methods based on the trade-off between accuracy and noise.

Detector response compensation in SPECT brain imaging, as in SPECT imaging in general, is complicated by the dependence of the detector response on the distance of the source from the detector. Stationary, deconvolution filter techniques, such as the Metz filter [21] are theoretically accurate only for a single distance from the detector and not for a distributed source. Theoretically more accurate techniques for detector response compensation have been proposd which model the distance-dependence [13], [15]. The primary disadvantage of these techniques is computational cost. In addition, it is questionable whether these more sophisticated approaches substantially improve absolute quantitative accuracy relative to the less time consuming approaches. This study addresses that question by comparing the quantitative accuracy in images reconstructed using the FB and Metz filter method with those reconstructed using a 3D ML method which models the distance-dependent detector response.

The reconstruction methods were tested on simulated 3D brain data. The simulation approach was chosen in order to eliminate the uncertainty in the true radioisotope concentration which is inherent in experimental phantom studies. The simulation did not consider the complicating effects of partial volume and scatter. The reconstruction times for both methods were documented.

II. Methods

A. 3D Brain Data Simulation

The 3D brain data were generated from a 3D computer phantom originally designed to simulate cerebral blood

Manuscript received December 1, 1992; revised March 1, 1993. This research was supported by grant no. DE-FG05-91ER60894 awarded by the Department of Energy and in part by DOE grant no. DE-FG05-90ER75577, NIH grant no. R01-CA3354, awarded by the National Cancer Institute, and PHS grant no. S10-RR04176.

The authors are with the Department of Radiology, Duke University Medical Center, Durham, NC 27710.

IEEE Log Number 9208957.

flow for PET [22]. The phantom consists of 19 transaxial slices depicting the gray and white matter and cerebral ventricles in the normal human brain. The relative source concentrations in the gray matter, white matter, and ventricles of the phantom are 4 : 1 : 0, respectively. The phantom was derived from a set of T1 weighted spin-echo MRI slice images taken at 7 mm thickness to span the entire brain. An example slice of the phantom is shown in Fig. 1.

The projections of the phantom were simulated discretely modeling photon attenuation and distance-dependent detector response in 3D. The contribution of a source voxel to a projection bin was weighted by detector response and attenuation factors which were computed as follows. For each source voxel a detector response function was derived which was Gaussian with σ a function of the distance from the source voxel to the detector. The dependence of σ with distance was based on line source measurements in air at varying distances from a gamma camera with a high resolution collimator. The response function was sampled at the detector plane at approximately 1.6 mm intervals in two dimensions to obtain detector response factors. From each sample point on the detector, or projection bin, the attenuation factor was computed as the integral of the attenuation coefficient along the ray beween the source voxel and the projection bin. This was done by analytically solving for the path length from the center of the source voxel to the body boundary. The body boundary was obtained from the computer phantom, and the assumed attenuation coefficient was 0.15/cm. The projections of all source voxels were summed within each projection angle. Following this, 2×2 projection bin neighborhoods were summed which resulted in a sampling period of approximately 3.3 mm relative to the size of the normal human brain. Projections were simulated at 120 angles over 360°.

Using a Poisson random number generator, noise was added to the projection data after scaling the data to count levels representative of clinical ^{99m}Tc Ceretec brain studies. Examination of several clinical Ceretec studies revealed that a representative total counts in a 3.6 mm slice was approximately 300,000. Five independent noisy projection data sets were generated.

The degree to which the simulated data modeled experimental data was assessed using acquired projection images of the actual 3D brain phantom. The phantom was filled with approximately 45 mCi of ^{99m}Tc, and data were acquired in two non-overlapping energy windows, one centered on the ^{99m}Tc photopeak, 126 to 154 keV, and the other adjacent to and below the photopeak window, 100–125 keV. The data from the latter window were scaled by 0.4 and subtracted from the photopeak data for scatter compensation [23]. Data were acquired into 128×128 matrices with a 3.6 mm sampling period at 120 angles over 360 degrees. The total scan time was 1 h. This high count study was designed to reduce noise effects. Fig. 2 shows the experimental and simulated noise-free projection images with profiles and illustrates the degree of similarity in the data sets.

Fig. 1. Single slice of 3D Hoffman brain phantom.

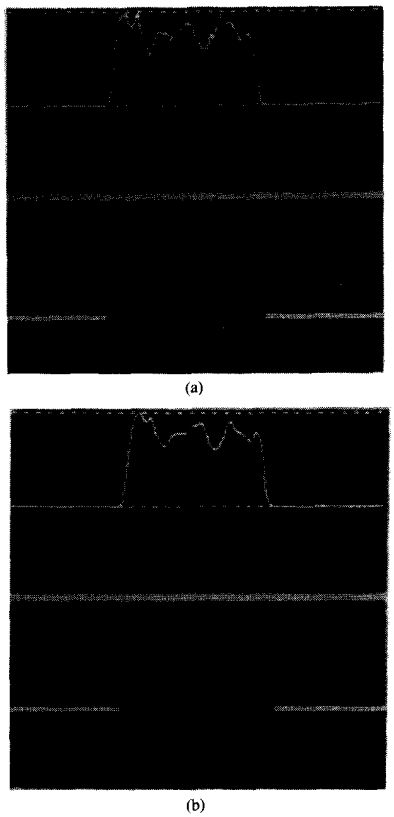

(a)

(b)

Fig. 2. (a) Experimental and (b) simulated noise-free projection images of 3D brain phantom with profiles.

B. Reconstruction Methods

Filtered Backprojection: The filtered backprojection (FB) reconstruction technique incorporated Metz filtering [21] for detector response compensation and the Chang algorithm [2] for attenuation compensation. A 2D Metz filter was applied to the projection data before reconstruction.

The MTF in the filter formula was a Gaussian, and the σ of the Gaussian was selected to match the detector response at the radius of rotation (15 cm). Based on the line source measurements at this distance, σ was determined to be 0.35 cm (FWHM equaled 0.82 cm). A range of filter powers for the Metz filter was tested which included 6, 12, 20, 30, and 50. The 1D Metz filter with power equal to 12 is shown in Fig. 3.

Chang attenuation compensation was applied in its single iteration form [2]. The body boundary was determined from the computer phantom. The attenuation coefficient was assumed 0.15/cm.

3D Maximum Likelihood-EM: The detection probabilities for the ML-EM algorithm modeled attenuation and detector response in 3D. There were two differences in the physical models of the reconstruction and data simulation. First, the sampling period in the reconstruction was a factor of two greater than in the data simulation. Second, the attenuation factors computed for the reconstruction considered attenuation integrals only along rays perpendicular to the detector plane. This simplification allowed a substantial reduction in memory requirements and processing time. The reconstruction model is inaccurate to the extent that the attenuation integral changes within the collimator acceptance angle for a fixed distance from the collimator. Since with high resolution collimators this angle is roughly two degrees, this error should be relatively small.

The attenuation coefficient for the 3D ML-EM algorithm was assumed 0.15/cm. A range of iteration stopping points was tested which included 50, 100, 150, 200, and 300.

C. Image Analysis

The quantitative accuracy relative to the actual phantom intensities and noise were evaluated in the reconstructed images in the gray and white matter regions separately. As a measure of quantitative accuracy the absolute value of the percent bias of reconstructed voxel intensities was computed, where,

$$\%\ \text{bias} = \frac{1}{N} \times \sum_{i=1}^{N} (f_i - phan) \times \frac{100}{phan}$$

where N is the number of voxels, f_i is the reconstructed intensity at voxel i, and *phan* is the phantom intensity in the particular region. As a measure of noise, the absolute value of the % standard deviation of reconstructed voxel intensities was computed, where

$$\%\ \text{stand. dev.} = \sqrt{\frac{1}{N} \sum_{i=1}^{N} (f_i - f_{mean})^2} \times \frac{100}{phan}$$

where f_{mean} is the mean of the reconstructed voxel intensities in the particular region.

The percent bias and standard deviation were computed for each method based on the entire gray or white matter regions in 10 reconstructed images. This included two separate transaxial slices reconstructed from each of five independent projection data sets. The numbers of gray and white matter voxels included in each computation was approximately 4000 and 2000, respectively. Including such a large number of voxels provided good estimates of the true bias and standard deviation. The percent bias and standard deviation were also computed for each method in reconstructed images of noise-free data. In order to illustrate the trade-off between quantitative accuracy and noise, the percent absolute bias is plotted versus percent absolute standard deviation for FB with varying Metz filter power and for ML with varying iteration number.

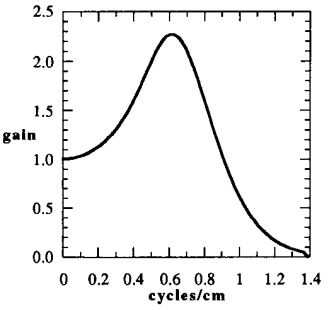

Fig. 3. Metz filter at power 12.

III. Results

The bias/standard deviation plots are shown in Fig. 4(a) for the gray matter region and Fig. 4(b) for the white matter region. The noise-free results have also been included in the plots. It should be noted that the signs of all bias measurements in the gray matter region were negative and in the white matter region were positive. From right to left in these plots the ML iteration number and FB Metz filter power increase. The noisy data plots show that as both the FB Metz filter power and the ML iteration number increase, bias decreases and standard deviation increases. Comparison of the FB and ML curves from noisy data shows that the ML curve lies below or to the left of the FB curve; the ML had smaller standard deviation than FB Metz for any given bias. (However, it does appear that in the gray matter region, for ML iterations less than 50, the reverse is true.) The ML method achieved a lower bias than FB in the gray matter region while the reverse is true in the white matter region.

The noise-free plots in Fig. 4 separate the contribution of the underlying signal to the reconstructed bias and standard deviation. In these plots the percent standard deviation is not the result of random noise in the data, but rather is due to a systematic artifact in the reconstruction. Such artifact could result, for example, from inaccurate compensation for the detector response or attenuation. In the white matter plot of Fig. 4(b), the noise-free FB reconstruction shows a substantially elevated percent

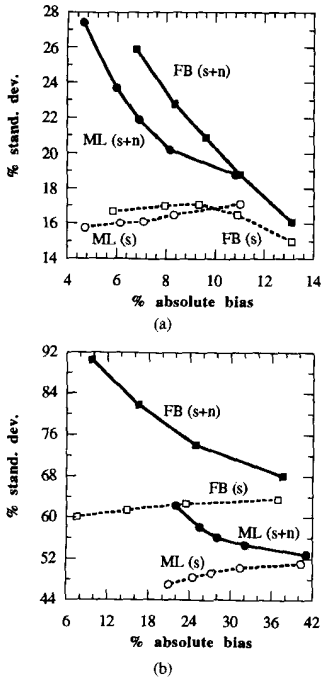

Fig. 4. Bias/standard deviation plots ($s + n$) refers to noisy data. (s) refers to noise-free data. (a) Gray matter region. From right to left ML data points are 50, 100, 150, 200, and 300 iterations, and FB data points are Metz filter powers 6, 12, 20, 30, and 50. (b) White matter region. From right to left ML data points are 50, 100, 150, 200, and 300 iterations, and FB data points are Metz filter powers 6, 12, 20, and 30.

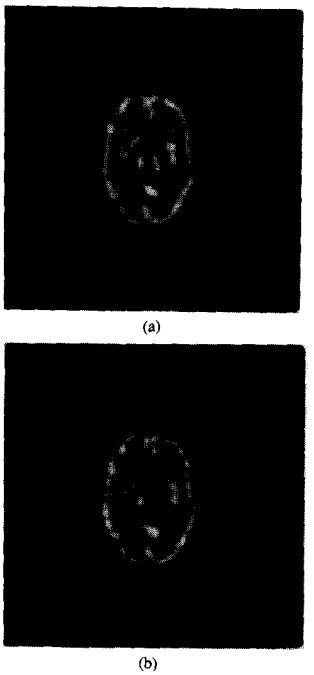

Fig. 5. Example reconstructions of simulated 3D brain phantom data. (a) Filtered backprojection (Metz = filter power = 12). (b) ML-EM, 100 iterations.

standard deviation relative to the ML reconstruction. This result suggests that the superior performance of ML with noisy data in this region may not be due to how the two methods handle random noise but rather to how they reconstruct the underlying signal.

Example reconstructed images from the two methods are shown in Fig. 5. Qualitative differences are apparent in the images. In particular, the ML image appears to have better resolution near the periphery of the brain than near the center.

IV. Discussion

This study compares ML and FB in terms of the trade-off between quantitative accuracy and noise as the respective reconstruction parameter varies (iteration number for ML, Metz filter power for FB). The study showed that the ML method had a smaller standard deviation than FB for a given bias. While it is difficult to generalize these results to other types of data, it appears that for brain imaging this implementation of ML could provide more accurate quantitation measurements than a similar FB algorithm.

The superior performance of the ML method may be the result of a more accurate model of the detector response. In the ML implementation for this study, the detection probabilities [17], [18] incorporate the distance-dependence of the detector response. The Metz filter, on the other hand, models the detector response assuming a constant distance from the detector. In brain studies such as the data presented here, where the structures of interest are close to or smaller than the width of the detector response function, detector response compensation can substantially affect quantitative accuracy.

A primary disadvantage of ML-EM relative to filtered backprojection is the greater processing time, and ways of reducing this processing time have been proposed [24]–[26]. In this study, the 3D ML-EM algorithm was implemented to optimize computational speed in a number of ways. First of all, the attenuation and detector response factors were precomputed and stored in memory for fast computation. Also, only a pre-defined source range was reconstructed rather than an entire $128 \times 128 \times 128$ reconstruction matrix. To reduce the memory requirements of this approach, scatter was not considered in the reconstruction and only non-negligible detection probabilities were stored in memory. A pre-defined source range also reduced memory requirements. Finally, by considering only the perpendicular attenuation factors, memory requirements were greatly reduced since a single attenuation factor could be applied for a number of source voxel/projection bin interactions.

Benchmark tests with the algorithm have been performed on a SUN SPARC II workstation. With 3.5 mm

sampling in 3 dimensions (typical of 128×128 acquisitions) 75,000 voxels were required to reconstruct the entire brain phantom. With this many voxels and 120 projection angles, the time per iteration was approximately 6 min and 40 M bytes of memory required. Preliminary experience with the HP 730 workstation indicates that the time per iteration can be reduced to approximately two minutes. The expected time per iteration with this implementation scales approximately linearly with the number of voxels.

REFERENCES

[1] S. Bellini, M. Piacentini, and C. Cafforio, "Compensation of tissue absorption in emission tomography," *IEEE Trans. Acoust. Speech Sig. Process.*, vol. 27, pp. 213–218, 1979.

[2] L. Chang, "A method for attenuation correction to radionuclide computed tomography," *IEEE Trans. Nucl. Sci.*, vol. NS-25, pp. 638–643, 1978.

[3] C. E. Floyd, R. J. Jaszczak, and R. E. Coleman, "Inverse Monte Carlo: A unified reconstruction algorithm for SPECT," *IEEE Trans. Nucl. Sci.*, vol. NS-32, pp. 779–785, 1985.

[4] G. T. Gullberg and T. F. Budinger, "The use of filtering methods to compensate for constant attenuation in SPECT," *IEEE Trans. Biomed. Eng.*, vol. BME-28, pp. 142–157, 1981.

[5] G. T. Gullberg, R. H. Huesman, and J. A. Malko, "An attenuated projector-backprojector for iterative SPECT reconstruction," *Phys. Med. Biol.*, vol. 30, pp. 799–815, 1985.

[6] R. J. Jaszczak, L. Chang, N. A. Stein, and F. E. Moore, "Whole body single photon emission computed tomography using dual large field-of-view scintillation cameras," *Phys. Med. Biol.* vol. 24, pp. 1123–1143, 1979.

[7] R. J. Jaszczak, R. E. Coleman, and F. R. Whitehead, "Physical factors affecting quantitative measurements using camera-based single photon emission computed tomography (SPECT)," *IEEE Trans. Nucl. Sci.*, vol. NS-28(1), pp. 69–80, 1981.

[8] M. A. King, R. B. Schwinger, B. C. Penney, *et al.*,"Digital restoration of indium-111 and iodine-123 SPECT images with optimized Metz filters," *J. Nucl. Med.*, vol. 27, pp. 1327–36, 1986.

[9] M. A. King, B. C. Penney, and S. J. Glick, "An image-dependent Metz filter for nuclear medicine images," *J. Nucl. Med.*, vol. 29, pp. 1980–1989, 1988.

[10] S. H. Manglos, R. J. Jaszczak, and C. E. Floyd, "Nonisotropic attenuation in SPECT: phantom tests of quantitative effects and compensation techniques," *J. Nucl. Med.*, vol. 28, pp. 1584–91, 1987.

[11] E. Tanaka, "Quantitative image reconstruction with weighted backprojection for single photon emission computed tomography," *J. Comp. Assist. Tomo*, vol. 7, pp. 692–700, 1983.

[12] O. J. Tretiak and C. E. Metz, "The exponential Radon transform.," *J. Appl. Math.*, vol. 39, pp. 341–354, 1980.

[13] B. M. W. Tsui, H. B. Hu, D. R. Gilland, and G. T. Gullberg, "Implementation of simultaneous attenuation and dector response correction in SPECT," *IEEE Trans. Nucl. Sci.*, vol. 35, pp. 778–783, 1988.

[14] T. E. Walters, W. Simon, D. A. Chesler, and J. A. Correia, "Iterative convolution for radionuclide axial tomography with correction for internal absorption," in *Reconstruction tomography in diagnostic radiology and nuclear medicine*, Ter-Pogossian MM, Phelps ME, eds., University Park Press, Baltimore, pp. 309–314, 1977.

[15] G. L. Zeng, G. T. Gullberg, B. M. W. Tsui, and J. A. Terry, "Three-dimensional iterative reconstruction algorithms with attenuation and geometric points response correction," *IEEE Trans. Nucl. Sci.*, vol. 38, pp. 693–702, 1991.

[16] C. E. Floyd, R. J. Jaszczak, K. L. Greer, and R. E. Coleman, "Brain phantom: High-resolution imaging with SPECT and I-123," *Radiology*, vol. 164, pp. 279–281, 1987.

[17] K. Lange and R. Carson, "EM reconstruction algorithms for emission and transmission tomography," *J. Comp. Assist. Tomo*, vol. 8, pp. 306–316, 1984.

[18] L. A. Shepp and Y. Vardi, "Maximum likelihood reconstruction for emission tomography," *IEEE Trans. Med. Imag.*, vol. MI-1, pp. 113–122, 1982.

[19] D. Snyder and M. Miller, "The use of sieves to stabilize images produced with the EM algorithm for emission tomography," *IEEE Trans. Med. Imag.*, vol. MI-10, pp. 3864–3870, 1985.

[20] E. Veklerov and J. Llacer, "Stopping rule for the MLE algorithm based on statistical hypothesis testing," *IEEE Trans. Med. Imag.*, vol. MI-6, pp. 313–319, 1987.

[21] C. E. Metz, "A mathematical investigation of radioisotope scan image processing," Ph.D. dissertation. University of Pennsylvania, 1969.

[22] E. J. Hoffman, P. D. Cutler, W. M. Digby, and J. C. Mazziotta, "3-D phantom to simulate cerebral blood flow and metabolic images for PET," *IEEE Trans. Nucl. Sci.*, vol. 37, pp. 616–620, 1990.

[23] R. J. Jaszczak, K. L. Greer, C. E. Floyd, C. C. Harris, and R. E. Coleman, "Improved SPECT quantification using compensation for scattered photons," *J. Nucl. Med.*, vol. 25, pp. 893–900, 1984.

[24] T. Herbert, R. Leahy, and M. Singh, "Fast MLE for SPECT using an intermediate polar representation and a stopping criterion," *IEEE Trans. Nucl. Sci.*, vol. 35, pp. 615–619, 1988.

[25] B. C. Penney, M. A. King, and K. Knesaurek, "A projector, back-projector pair which accounts for the two-dimensional depth and distance dependent blurring in SPECT," *IEEE Trans. Nucl. Sci.*, vol. 37, pp. 681–686, 1990.

[26] G. L. Zeng and G. T. Gullberg, "Frequency domain implementation of the three-dimensional geometric point response correction in SPECT imaging," *IEEE Trans. Nucl. Sci.*, vol. 39, pp. 1444–1453, 1992.